Direct micro-imaging of point defects in bulk SiO$_2$, applied to vacancy diffusion and clustering

E. Suhovoy, V. Mishra, M. Shklyar, L. Shtirberg and A. Blank[(a)]

Schulich Faculty of Chemistry, Technion, Israel Institute of Technology - Haifa, 32000, Israel

Abstract – Electron spin resonance microscopy (ESRM) was employed in the evaluation of diffusion characteristics of point defects (E$'$ paramagnetic centers) in amorphous SiO$_2$. Samples were subjected to inhomogeneous γ-irradiation creating a heterogeneous distribution of E$'$-centers in SiO$_2$ substrates. The samples were measured by ESRM after preparation and following several heat treatment cycles. These measurements revealed pronounced changes in the distribution of the E$'$-centers due to the heat treatments. The defects' reorganization did not obey simple diffusion laws and they exhibited an attraction towards areas with higher initial concentration. This behavior was simulated by an empirical model, resulting in the evaluation of the defects' diffusion constant, its activation energy, and their characteristic attractive potential. This is the first time that ESR imaging is employed to directly obtain such type of fundamental information regarding the diffusion behavior and interaction of point defects.

Introduction. – The performance of many semiconductor devices depends upon the unique physical properties of the semiconductor material and the oxide layers. For example, typical MOSFET semiconductor transistors are manufactured from silicon (Si) and silicon dioxide (SiO$_2$), whose properties, such as energy band structure and charge carrier mobility, are very sensitive to crystal imperfections. Due to the importance of defects in the field of materials science and specifically in semiconductors, many efforts have been invested in developing methodologies to observe these structures. In principle, defects can be detected either indirectly, through their effects on the semiconductor's physical/electrical properties, or directly using 3D imaging. The physical/electrical activity of the defects can be detected and characterized by techniques such as electron spin resonance (ESR) [1], nuclear magnetic resonance (NMR) [2], deep-level transient spectroscopy (DLTS) [3], and thermally stimulated current (TSC) analysis [4]. For large enough samples with a macroscopic homogeneous nature, these types of measurements can be used to detect even low densities of electrically active defects (introducing levels into the forbidden energy gap). However, this information, without knowledge of the 3D defect distribution, is often insufficient. The

defects' structural nature can be characterized by transmission electron microscopy (TEM) [5] and various X-ray diffraction methods for detecting lattice imperfections [6]. The TEM technique provides excellent 2D resolution, but requires a special sample preparation and the interpretation of the results is often not straightforward. In addition, it cannot detect small, sporadic defects, especially *point defects or single vacancies* [7]. The X-ray diffraction techniques are also insensitive to low defect densities and can produce only 2D images. The low-energy X-ray microscopy method (NEXAFS-SPXM) can be used to achieve 3D images with a resolution down to 10 nm; however, it works only in samples having a relatively low atomic number, a thickness of less than 200 nm, and again, is sensitive only to major defects (as opposed to point defects) generating structural anomalies in the nanometer scale [8]. Another possibility to indirectly look at point defects is by using doping metals such as gold, platinum or zinc that tend to settle in crystal vacancies and subsequently can be imaged at high resolution by electron microscopy or secondary ion mass spectrometry (SIMS) methods. This doping approach has many limitations and associated problems, as discussed in ref. [9].

As a result of these deficiencies, several important properties and materials characteristics cannot be *directly* measured at present. For example, diffusion and clustering

---

[(a)]E-mail: ab359@tx.technion.ac.il

of point defects in the bulk, which do not exhibit fluorescent signals (and/or are in non-transparent materials), cannot be measured experimentally in a *direct* manner [9,10]. (In the case of surface defects, scanning tunneling microscopy (STM) can be used to observe the diffusion of vacancies in real time and extract information about their diffusion coefficient, activation energy, and jump rate [11,12]. In the case of fluorescent point defects, optical microscopy can extract the diffusion data based on their images at different times, starting from an inhomogeneous artificially generated pattern [13].) Point-defect diffusion and clustering plays a crucial role in many aspects of semiconductor devices. For example, when dopant impurities are implanted, the resulting implant damage leads to point-defect supersaturation. Dopant diffusion is greatly affected by point-defect concentration; therefore, dopants are subjected to transient enhanced diffusion (TED) until the point defects have diffused to their equilibrium distribution [14]. Thus, the capacity to control device profiles is crucially dependent on the ability to model in a quantitative way the motion and annealing of point defects [15]. This type of information is also important, for example, in numerical programs dealing with device-processing simulation. Furthermore, since the diffusion and reorganization of point defects can also be mediated by their concentration, due to some mutual interaction mechanism, it can also help to understand the properties and the sources of forces operating within the crystal and between defects (as shall be shown here).

In this work we follow a common approach for measuring the diffusion of defects, trying to generate a "step function" in their concentration and subsequently monitoring their reorganization under controlled temperature and time. However, as noted above, unlike previous similar efforts, we *directly* monitor the point defects themselves by employing a state-of-the-art ESR micro-imaging technique. This is done in order to image defects in amorphous SiO_2 (so called E'-centers) with a resolution that is sufficient to observe their unique diffusion behavior (including mutual interaction) and also estimate the diffusion activation energy. These types of point defects play an important role in determining the electronic properties of the near Si/SiO_2 interface dielectrics, affecting also the properties of the bulk SiO_2. For example, leakage currents have been linked to the existence of these centers [16], and they are also considered to be a dominant hole trap, thus affecting device performance. As noted above, up until now, no *direct* experimental technique could monitor the diffusion and re-organization of such defects, thus limiting the scope of the existing relevant research.

Experimental. – The ESR micro-imaging system used in this work was described in details in reference [17] and the referenced documents therein. In brief, it is a home-made pulsed system operating at 17 GHz and equipped with a miniature and sensitive imaging probe. The probe is based on a single ring microwave resonator machined from a TiO$_2$ (rutile) single crystal surrounded by
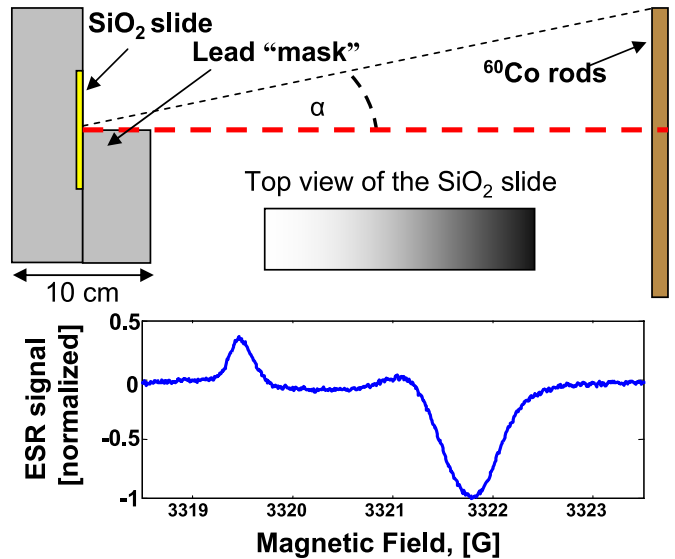

Fig. 1: (Colour on-line) Top: the experimental set-up used for generating a gradient of paramagnetic defects in the SiO$_2$ slide. The top view of the slide shows the ideal distribution of defects following such kind of irradiation. (In practice, more complex patterns were generated due to limitations in irradiation set-up and the clustering properties of the defects.) Bottom: continuous wave ESR spectrum of the irradiated SiO$_2$ slides. Acquisition parameters: microwave frequency = 9.316 GHz; power = 0.63 mW; modulation frequency = 100 kHz; modulation amplitude = 0.1 G.

high-efficiency miniature gradient coils. The permittivity of this crystal is high (anisotropic with values of 165 and 85 at room temperature), which results in small dimensions of o.d. = 2.4 mm, i.d. = 0.9 mm and a height of 0.5 mm (for $\sim$17 GHz resonance frequency). At room temperature it demonstrated spin sensitivity of $\sim 3 \times 10^6$ spins (for acquisition time of $\sim$1 hour and samples with a linewidth of $\sim$0.1 G), and image resolution that is slightly better than $1 \mu m$ (for a high-spin concentration sample with $\sim 10^8$ spins per $[1 \mu m]^3$).

Samples of amorphous SiO$_2$ with an inhomogeneous distribution of E' point defects were prepared by subjecting 250 μm thick quartz cover slips (from Specialty Glass Products, PA, USA) to γ-irradiation from a ^{60}Co source (carried out at the "Nahal Sorek" facility, Yavneh, Israel) through a lead "mask", in the manner described in fig. 1 (top). Ideally, the lead "mask" should have shielded only one half of the slide from radiation. In practice, due to the large thickness required to shield from the intense γ-irradiation (5 cm reduces the energy by $\sim$99%) and the unavoidable deviation of the α angle from 0, the resulting defects pattern could not be very sharp (but still good enough for our experimental needs). The identification and quantification measurements of the E'-centers were carried out by a conventional continuous wave (CW) ESR system (Bruker EMX system, at 9 GHz).

Results. – Figure 1 (bottom) shows a typical CW ESR spectrum of one of the irradiated SiO$_2$ samples.
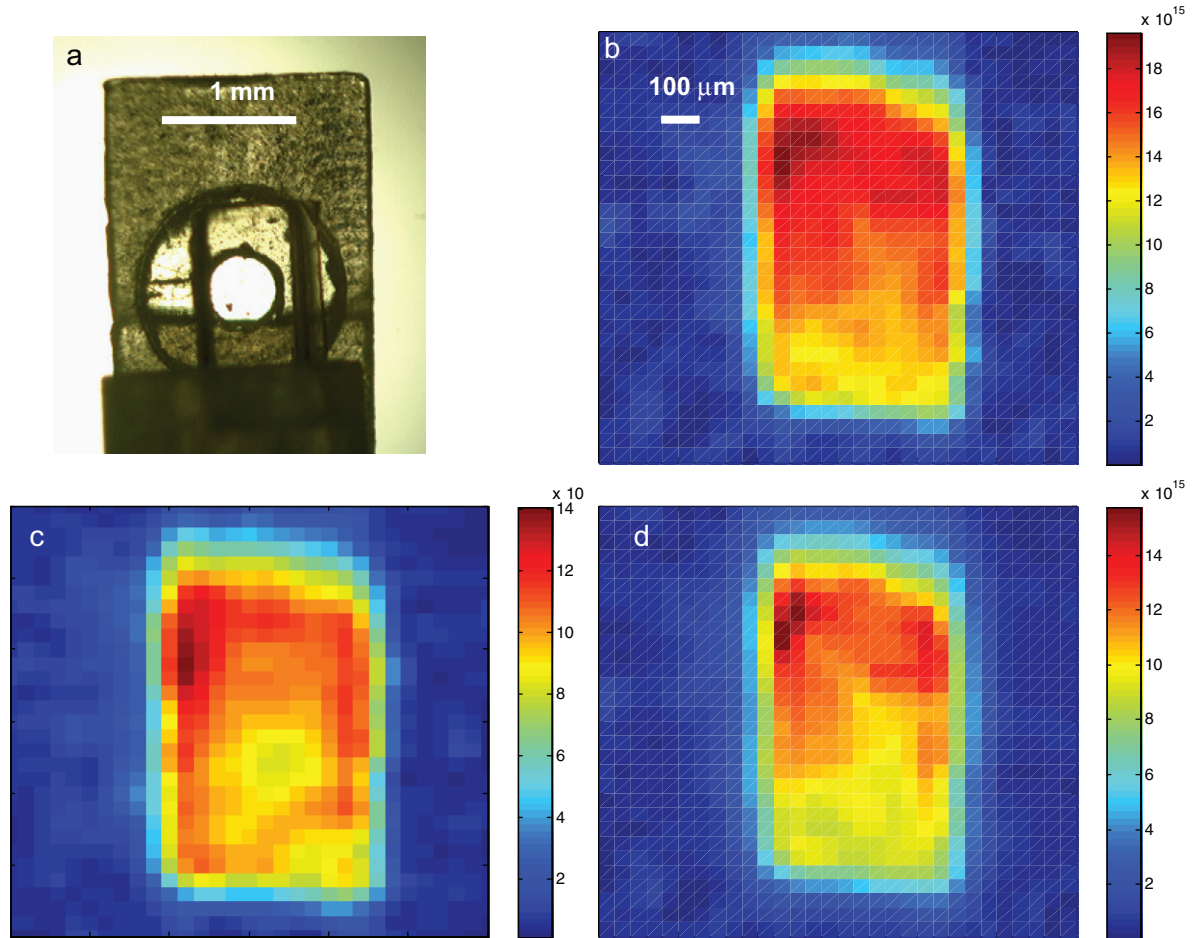
Fig. 2: (Colour on-line) (a) An optical image of a typical $\sim 1 \times 2$ mm SiO$_2$ piece placed above the ESR resonator during the imaging experiments. (b) ESR image taken after the irradiation. (c) The same as (b) but after a 12 h heat cycle at 100 °C. (d) Simulated results based on the initial image (b) that predict the distribution of the defects following the 12 h heat treatment. The best-fit parameters are listed in table 1. The vertical color scale corresponds to the concentration of defects in an arbitrary but consistent scale for all ESR images.

The spectrum is characteristic of E$'$-centers in amorphous SiO$_2$, as described in the literature [16,18–20]. (It should be noted that the common nomenclature in the literature relates to E$'$-centers as oxygen vacancy both in amorphous and crystal SiO$_2$, as they are indistinguishable by their ESR signal [21].) The concentration of the paramagnetic centers in the section of the sample that was fully affected by γ-irradiation was determined by comparing its double integral CW signal to the signal of a reference sample (a 1 μM trityl radical solution with a known number of spins) and it was found to be 3.6×10^{14} spins/cm^3.

Following the irradiation procedure, the cover slips were sliced into rectangular pieces of either 1×20 or 1×2 mm and inserted into the ESR imaging probe for imaging (see fig. 2(a)), with the long side of the slices always along the irradiation gradient. Due to the relatively limited instantaneous field of view of the imaging probe (~ 1 mm in diameter), the rectangular slices were imaged at two (for the 2 mm long slides) or three (for the 20 mm long slides) different locations around their center. This allowed a more complete view of the irradiated zone near the

"light"/"shadow" transition region. The 2D resolution of all ESR images was $\sim 40 \, \mu$m. After each imaging session, the sliced rectangular pieces were inserted into a temperature-controlled laboratory oven for a heat cycle of 6 to 12 hours at a specified temperature within the range of 50–100 °C.

Figures 2(b) and 2(c) show typical ESR images of a 1×2 mm SiO$_2$ piece prior to and following 12 hours of heat treatment at 100 °C. The inhomogeneous distribution of defects is apparent both before and especially after the heat treatment. Figures 3(a)–(c) provide another examples of defect distribution before and after heat treatment, measured in a small sector that covers part of a 2×20 mm sample (near its center). It is clear from these representative results that heat treatment affects defect distribution in several manners. First, the overall signal (proportional to the defects' concentration) decreases. This can be attributed to partial annealing of the defects that is known to occur in irradiated SiO$_2$ samples at elevated temperatures [19]. Second, the spins' spatial distribution changes in a non-trivial manner that can be
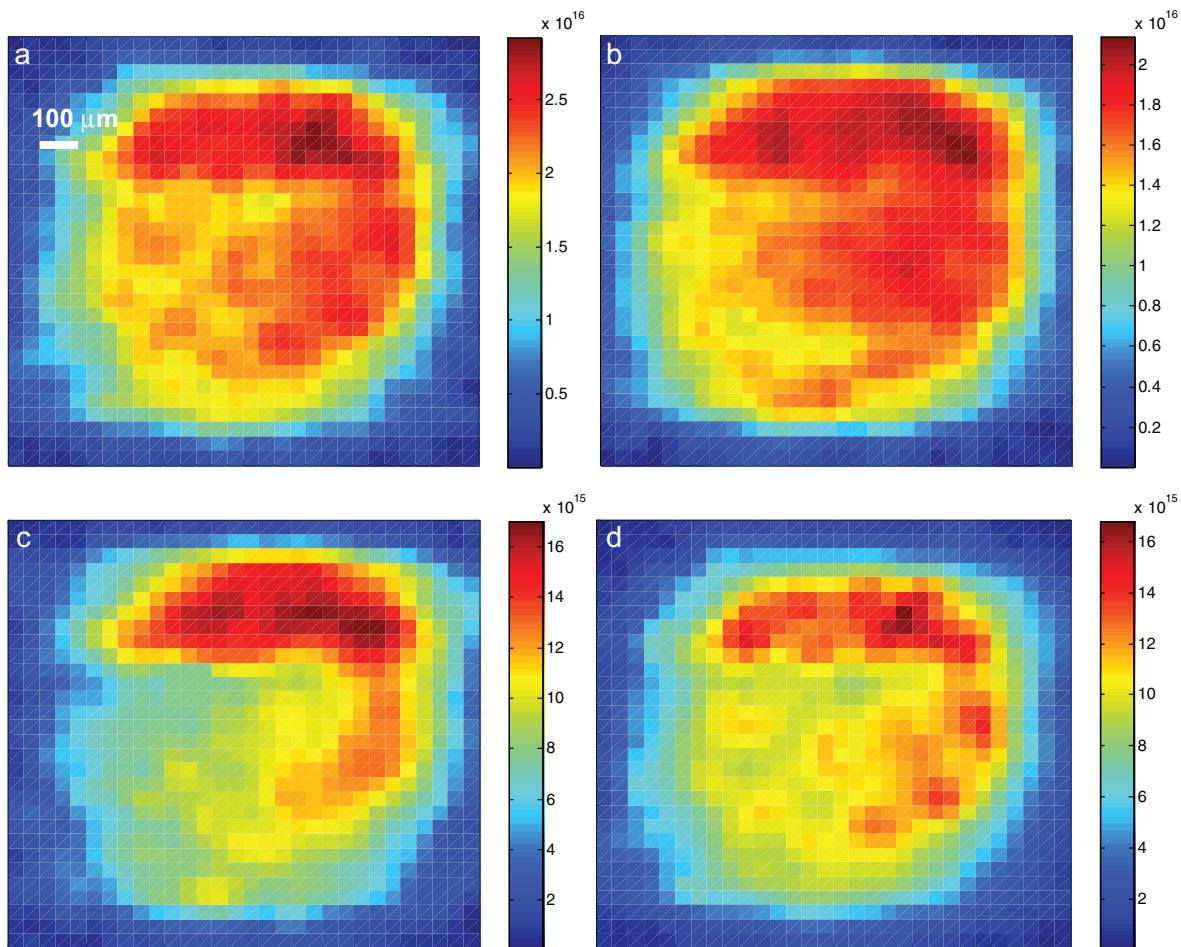
Fig. 3: (Colour on-line) (a) An ESR image covering part of a typical $\sim 2 \times 20$ mm SiO$_2$ piece taken after the irradiation. (b) Same as (a) but after a 12 h heat cycle at 50 °C. (c) Same as (a) but after a 12 h heat cycle at 100 °C. (d) Simulated results based on the initial image (a) that predict the distribution of the defects following the 12 h heat treatment at 100 °C.

described as a combination of simple diffusion along with a tendency of the defects to accumulate near areas with higher initial concentrations (clustering).

In view of the above, an empirical model was formulated in order to simulate the unique type of defect reorganization observed in our measurements. In the model, the diffusion part was considered according to Fick's first law, resulting in defect flux from regions of high concentration to regions of low concentration. However, since simple diffusion alone could not explain the measured change in spin distribution, a simple attraction between collections of defects was considered in the model. In mathematical terms, the following equations were assumed to govern the re-organization of the defects. The flux of defects in the presence of concentration gradient and force is described by a special case of the Fokker-Planck equation [9]:

$$J_{\vec{r}} = -D \cdot \frac{\partial C}{\partial \vec{r}} + D \cdot C \cdot \frac{F_{\vec{r}}}{k_B T}, \tag{1}$$

where $J_{\vec{r}}$ is the flux of defects, D is the diffusion coefficient, C is the concentration of defects, $\vec{r}$ is the distance vector along a specific direction for which the flux and force, $F_{\vec{r}}$, are calculated, k_B is the Boltzmann constant, and

T is the temperature. In addition to the flux equation, the decrease of defects concentration due to annealing is typically described as first-order kinetic process by the following equation:

$$\frac{\partial C}{\partial t} = -k_a C, \tag{2}$$

where k_a is the annealing constant. The force is assumed to behave according to the following empirical expression: $F_{\vec{r}} = k_F \cdot C_i \cdot C_j \cdot |\vec{r}_i - \vec{r}_j|^{-4}$ where k_F is a force constant, C_i and C_j are the concentrations of defects in two different locations, resolved by the image that the force acts between them, and $|\vec{r}_i - \vec{r}_j|$ is the distance between these two different locations. The rationale behind this type of force behavior is mainly empirical (*i.e.* it reproduces the migration of the defects —as shall be shown below), but it can also be linked to more fundamental theoretical work (as shall be described in the Discussion section).

Equations (1), (2) can be solved numerically to obtain the expected pattern of defects as a function of time, based on the initial condition of the defects' distribution at time 0. The defects' distribution is propagated over time in several iterations to reach the simulated image that should

Table 1: Summary of the experimental and simulated results presented in figs. 2, 3: the first column lists the initial condition image of the spins' distribution prior to the relevant heat cycle (this is an experimental result). The second column relates to the image of the spins' distribution after the relevant heat cycle (also an experimental result). The third column provides the image of the spins' distribution after the relevant heat cycle (simulated result, based on the initial condition image). The forth and fifth columns provide the temperature and time duration of the heat cycle treatment, respectively. The sixth and seventh columns give the fitted diffusion coefficient of the defects and the force constant between the defects (see eq. (1)), respectively. Finally, the eighth column lists the interaction attraction energy between two collections of defects having typical concentration of 10^{16} spins/m^2 (*e.g.*, 1.6×10^7 spins per resolution pixel in the image), located at a distance of $40\,\mu$m (the image resolution).

Init. cond. (exp)	After heat (exp)	After heat (sim)	T (K)	Time (h)	D (m^2/s)	k_F (J·m^7)	E (eV)
fig. 2(b)	fig. 2(c)	fig. 2(d)	373	12	4.1×10^{-15}	0.25×10^{-64}	0.24
fig. 3(a)	fig. 3(b)	Not shown	323	12	2×10^{-15}	0.007×10^{-64}	0.0068
fig. 3(b)	fig. 3(c)	fig. 3(d)	373	12	4×10^{-15}	0.17×10^{-64}	0.16

correspond to the measured defects' distribution after heat treatment. This simulated image depends on three fitting parameters, the diffusion (D), the force constant (k_F), and the annealing constant (k_a). The last parameter can be extracted with good accuracy quite independently of the other two parameters. This leaves only two fitting parameters at hand that can be optimized by comparing the simulation results to the experimental images. A linear least-square optimization was used in order to find the best set of D and k_F values that would match the experimental results. The comparison between the experimental and simulation results is presented in figs. 2 and 3. Table 1 summarizes the fitted D and k_F values for figs. 2 and 3, along with some experimental parameters and the simulated energy of interaction between the defects (see discussion for more details).

Discussion. – The oxygen vacancies' diffusion coefficients we obtained from the simulation fitting are in the order of $\sim10^{-15}$–10^{-14} m^2/s (table 1). As noted above, there are many complexities associates with the measurements of this parameter, and we could not find any previous experimental work describing this property in SiO$_2$ (crystal or amorphous) with which to compare our results. One possible point of reference can be obtained by looking at experimental work carried out with vacancies in pure Si. Here, a variety of indirect methods resulted in an abundance of data [9]. In the temperature range used in our work (~373 K), typical diffusion coefficient values for vacancies in Si were found to be $\sim10^{-12}$–10^{-13} m^2/s. Keeping in mind that diffusion coefficients in condensed matter tend to spread over many decades [10], the differences between the Si data and our SiO$_2$ data are reasonable and support the validity of our approach. Another option to try and compare the present results with prior work is to look at the activation energy of the diffusion (sometimes denoted as migration enthalpy). Our results with heat treatments at 50 and 100 °C (fig. 3 and table 1) can be used to roughly estimate the activation energy for the E'-centers diffusion to be ~0.14 eV. Again, this can be compared to the experimental work in pure Si, which has found a migration enthalpy of ~0.12–0.3 eV for various types of vacancies in a temperature range similar to that used in our present work [9]. As for theoretical work, one

can find some remotely relevant citations with calculations that are mainly directed towards the prediction of the formation rather than the migration enthalpy. The former, with typical bulk matter values of a few eV, often tends to be much higher than the latter, with typical values of few tenths of eV [9]. For example, recent efforts based on first-principles calculations and empirical potential molecular dynamics found in amorphous SiO$_2$ a distribution of formation enthalpy for oxygen vacancies centered around 5.52 eV with standard deviation of 0.3 eV. There is no theoretical work for the migration enthalpy, but clearly it should be much lower than the formation energy; otherwise, we could not have observed in the present work any measurable migration of defects in the relatively low temperatures we employed here.

As for the clustering phenomenon we observed, it requires more detailed discussion. Here we attempt to shed some light on the possible origins of this attractive interaction. In our experiments, the spin concentration was in the range of $\sim10^{14}$ spins per cm^3 (significantly less than the saturation E' concentration in SiO$_2$, which is around 10^{17} spins per cm^3 [18]). This means that the typical distance between vacancies was ~100–200 nm and most probably not less than ~50 nm. At such a relatively large distance, direct interaction between vacancies, other than electrostatic, seems unlikely. The literature on E'-centers mention the possibility of both positively charged and neutral E'-centers in quartz [21]. Here we observed an attractive interaction between the defects, so it seems safe to assume that the defects were not positively charged (and therefore repulsive), which again raises the question of the source of the clustering phenomenon we observed. Our attempted explanation relies on an indirect interaction between the vacancies that is mediated through the quartz structure, commonly known as "elastic interaction". Analytical models for elastic interaction were developed in the 1950s for point defects in the bulk with isotropic and cubic symmetry [22]. More recent results, based on similar formalism, were developed for thin films and 2D structures [23]. In the case of quartz crystal (considered here as a rough reference, although it is not amorphous), which has a cubic symmetry, one can find that the order of magnitude of the interaction energy between two defects separated by r is $\sim E_{\text{int}} = -(\frac{a_0}{r})^3$,

when E_{int} is expressed in eV and a_0 is the lattice constant [22]. For the quartz's 5 Å lattice constant we get a rather small value of $E_{int} \sim -10^{-6}$ eV for the interaction energy at a minimal expected distance of 50 nm. At this point we cannot offer a rigorous model that can bridge the gap from the microscopic picture of two interacting defects at a small distance to the macroscopic world of many spins interacting at longer length scales, as revealed by the ESR image resolution. Still, for a large collection of defects, whose number grows as r^3, the collective force that may be inflicted can be substantial and may be the source of the clustering phenomena we observed. Table 1 provides some quantitative information of relevance for the typical interaction energy found in the simulation, based on the force constant k_F. Our results seem to indicate that as temperature increases, a typical interaction energy of a few tenths of eV appears between two groups of $\sim 10^7$ spins at a typical distance of few tens of microns. In the future, a more elaborate theoretical analysis can and should be performed to better clarify both the microscopic picture and its relation to the macroscopic world. In that respect, the functional behavior of the force at both the microscopic (nm) and the macroscopic (μm) regimes can be proved to be much more complicated, but the bottom-line interaction energy should be in the order of what was found here. The theoretical analysis may also relate the interaction energy and force constant(s) to the migration enthalpy of the point defects and the crystal elastic properties. This future analysis may be compared to more accurate experiments in which the "initial conditions" of defects are generated by an accurate E-beam accelerator, resulting in much sharper "dark/light" boundaries. Furthermore, future work may also include ESR images with much better resolution, even in the sub-micron range, by using more defects concentrated samples and measuring them at higher magnetic fields and lower temperatures [17].

An additional point of importance is apparent in fig. 2(b) and even in a more pronounced manner in the same sample after heating (fig. 2(c), and simulated in fig. 2(d)). Here one can clearly see more defects accumulating near the sides of the slide, beyond the predictions of our clustering model. This phenomenon has also been observed in several other samples we measured and in previous 1D ESR imaging experiments of γ-irradiated SiO$_2$, carried out at lower resolutions [20]. This kind of behavior is another possible hint to the important role of elastic interaction that may lead to defect migration towards the edges of the sample with different strain conditions (this is not considered by our current empirical model).

$* * *$

REFERENCES

[1] Chen S. G., Branz H. M., Eaton S. S., Taylor P. C., Cormier R. A. and Gregg B. A., *J. Phys. Chem. B*, **108** (2004) 17329.

[2] Bromberger C., Jansch H. J., Kuhlert O., Schillinger R. and Fick D., *Phys. Rev. B*, **69** (2004) 245424.

[3] Cova P., Menozzi R., Portesine M., Bianconi M., Gombia E. and Mosca R., *Solid-State Electron.*, **49** (2005) 183.

[4] Pintilie I., Pintilie L., Moll M., Fretwurst E. and Lindstroem G., *Appl. Phys. Lett.*, **78** (2001) 550.

[5] Beanland R., *Ultramicroscopy*, **102** (2005) 115.

[6] Wang Y., Du X. L., Mei Z. X., Zeng Z. Q., Xu Q. Y., Xue Q. K. and Zhang Z., *J. Cryst. Growth*, **273** (2004) 100.

[7] Umeda T., Toda A. and Mochizuki Y., *Eur. Phys. J. AP*, **27** (2004) 13.

[8] Vearey-Roberts A. R., Steiner H. J., Evans S., Cerrillo I., Mendez J., Cabailh G., O'Brien S., Wells J. W., McGovern I. T. and Evans D. A., *Appl. Surf. Sci.*, **234** (2004) 131.

[9] Pichler P., *Intrinsic Point Defects, Impurities, and Their Diffusion in Silicon* (Springer, New York) 2004.

[10] Heitjans P. and Kärger J., *Diffusion in Condensed Matter: Methods, Materials, Models* (Springer, Berlin, New York) 2005.

[11] Kitamura N., Lagally M. G. and Webb M. B., *Phys. Rev. Lett.*, **71** (1993) 2082.

[12] Schaub R., Wahlstrom E., Ronnau A., Laegsgaard E., Stensgaard I. and Besenbacher F., *Science*, **299** (2003) 377.

[13] Martin J., Wannemacher R., Teichert J., Bischoff L. and Kohler B., *Appl. Phys. Lett.*, **75** (1999) 3096.

[14] Bracht H., Haller E. E. and Clark-Phelps R., *Phys. Rev. Lett.*, **81** (1998) 393.

[15] Eaglesham D. J., Venezia V. C., Gossmann H. J. and Agarwal A., *J. Electron Microsc.*, **49** (2000) 293.

[16] Lenahan P. M. and Mele J. J., *J. Vac. Sci. Technol. B*, **18** (2000) 2169.

[17] Blank A., Suhovoy E., Halevy R., Shtirberg L. and Harneit W., *Phys. Chem. Chem. Phys.*, **11** (2009) 6689.

[18] Agnello S., Boscaino R., Buscarino G. and Gelardi F. M., *J. Non-Cryst. Solids*, **345-346** (2004) 505.

[19] Jani M. G. and Halliburton L. E., *J. Appl. Phys.*, **56** (1984) 942.

[20] Sueki M., Eaton S. S. and Eaton G. R., *Appl. Radiat. Isot.*, **47** (1996) 1595.

[21] Fleetwood D. M., Pantelides S. T. and Schrimpf R. D., *Defects in Microelectronic Materials and Devices* (CRC Press, Boca Raton) 2009.

[22] Eshelby J. D., *Solid State Phys.*, **3** (1956) 79.

[23] Peyla P., Vallat A., Misbah C. and Muller-Krumbhaar H., *Phys. Rev. Lett.*, **82** (1999) 787.